The Dynamics of Disorder-Order Transitions in Hard Sphere Colloidal Dispersions

Paul M. Chaikin, Jixiang Zhu, Zhengdong Cheng
Department of Physics
Princeton University

See-Eng Phan and William B. Russel
Department of Chemical Engineering
Princeton University

Christian T. Lant, Michael P. Doherty,
William V. Meyer, Richard Rogers
NASA Lewis Research Center

D.S. Cannell
Department of Physics
UC Santa Barbara

R.H. Ottewill
School of Chemistry
Bristol University

PHaSE Team
Crew of Space Shuttle Columbia, STS-73
Crew of Space Shuttle Columbia, STS-83, STS-94

Abstract – The Physics of Hard Spheres Experiment (PHaSE) seeks a complete understanding of the entropically driven disorder-order transition in hard sphere colloidal dispersions. The light scattering instrument designed for flight collects Bragg and low angle light scattering in the forward direction via a CCD camera and performs conventional static and dynamic light scattering at 10-160° through fiber optic cables. Here we report on the kinetics of nucleation and growth extracted from time-resolved Bragg images and measurements of the elastic modulus of crystalline phases obtained by monitoring resonant responses to sinusoidal forcing through dynamic light scattering. Preliminary analysis of the former indicates a significant difference from measurements on the ground, while the latter confirms nicely laboratory experiments with the same instrument and predictions from computer simulations.

INTRODUCTION

The simplest colloidal dispersion consists of hard spheres, which interact through hydrodynamic and Brownian forces but feel no direct force before an infinite repulsion at contact. The hard sphere phase diagram, including the disorder-order transition, has been well established (Pusey & van Megen 1987), but many-body interactions complicate the understanding of the transport properties at higher concentrations in both disordered/metastable fluids and the ordered solid.

Recent studies of the kinetics of nucleation of nucleation and growth with colloidal hard spheres (Schatzel and Ackerson 1992, 1993; Harland, et al. 1995; He, et al. 1996; Harland and van Megen 1997) monitor either the small angle scattering that reflects the form factor for growing crystallites or the intensity, position, and width of the main interlayer Bragg reflection as a function of time. From these the amount of crystalline phase, the average linear dimension and number density of the crystallites, and the volume fraction within the crystallites are deduced. In the coexistence region the observations are compatible with the classic picture of sequential nucleation and growth of isolated crystals, though diffusion processes create a region around the growing crystallite at a lower concentration than the bulk fluid. Above melting nucleation events seem to become correlated, accelerated nucleation and suppressing growth. Coarsening begins as crystallization is completed, increasing the average crystallite size and reducing the number of crystallites. However, the process is quite complex and far from fully understood.

Most previous studies of rheological properties of hard spheres under both steady (Krieger 1972; Mewis, et al. 1989; van der Werff & deKruif 1989) and oscillatory shear (van der Werff, et al. 1989; Frith, et al. 1990; D'Haene, et al. 1992; Shikata & Pearson 1994) examined the fluid phase below the freezing transition and in the metastable region above. Many rheological studies also exists for colloidal crystals, but focus on aqueous dispersions dominated by electrostatic forces (Benzing & Russel 1981; Buscall, et al. 1982; Lindsay & Chaikin 1982; 1985; Chen, et al. 1994; Chow, et al. 1995; van der Vorst, et al. 1995). The main difficulty in determining the elasticity is that colloidal crystals are orders of magnitude weaker than conventional atomic solids and, thus, easily melt under shear. Oscillatory shear of small amplitude slightly perturbs the microstructure and is suitable for measuring the linear viscoelasticity of colloidal crystals.

Frenkel and Ladd (1987) computed the static elastic constants for hard sphere crystals from molecular dynamics simulations of slightly distorted unit cells at several concentrations and then averaged over all orientations to obtain the static shear modulus G'. Nunan and Keller (1984) calculated the orientation-dependent effective viscosity of periodic arrays of spheres in an incompressible Newtonian fluid and averaged over all orientations. Colloidal particles undergo Brownian fluctuations within the crystal lattice, whereas Nunan and Keller assumed the particles to be fixed on the lattice. Interactions at smaller separations imply a higher viscosity, so their predictions represent a lower bound.

Here we report the kinetics of nucleation and growth extracted from the time evolution of the main Bragg peak and rheological measurements for colloidal crystals of nonaqueous hard spheres by exciting shear waves and detecting the response via dynamic light scattering. The nucleation and growth data and the shear modulus and dynamic viscosity from experiments performed in microgravity on NASA space shuttle missions STS-83 and STS-94 are compared with simulations and models as well as measurements under normal gravity.

COLLOIDAL SPHERES

R.H. Ottewill and his group at University of Bristol synthesized and graciously supplied samples of poly-(methyl methacrylate) (PMMA) spheres with a grafted comblike layer of poly-(12-hydroxy stearic acid) (PHSA) chains that we dispersed in a refractive index matching mixture of 1,2,3,4-tetrahydronapthalene (tetralin, n=1.541) and 1,2,3,4-cis-decahydronaptha-lene (decalin, n=1.4815). Tetralin is a good solvent for PMMA and swells the particles, significantly increasing the size. Index matching suppresses the van der Waals forces and is necessary for performing light scattering, but the associated swelling increases the effective hard sphere volume fraction ϕ. The particle diameter from dynamic light scattering on a dilute sample is 655±15 nm. Previous measurements of the equation of state demonstrate them to be near hard spheres (Phan, et al. 1996). Polydispersity affects the freezing transition (Bolhuis & Kofke 1996), but the error in determining the concentration (±0.007) exceeds the correction for the 5% polydispersity of our samples. Thus, the effective volume fractions reported here do not include the effect of polydispersity.

EXPERIMENT

A multipurpose light scattering instrument was designed by NASA Lewis Research Center, ADF Corporation, NYMA Corporation, Titan Spectron, and Princeton University for the Physics of Hard Sphere Experiments or PHaSE (Lant, et al. 1997). This instrument performs both static and dynamic light scattering and also oscillates the sample for determining the rheological properties. Specially designed glass sample cells, whose refractive index (n=1.511) matches that of our PMMA-PHSA suspensions, consist of two pieces, a face plate and a hemispherical cap. The cap has a parabolic skirt and a cylindrical cavity, 10 mm in radius and 10 mm high, that requires approximately 3 mL of sample. The face plate is screwed into the cap to seal the sample. To allow for expansion and contraction due to temperature fluctuations, we incorporate a rubber diaphragm in the sample cell. All surfaces of the sample cell are highly polished and coated with anti-reflective material.

A 100 mW Adlas diode laser Model DPY313II supplies a 532 nm green beam, which is split into two, one for static light scattering and the other for dynamic. Each beam is routed with Newport mirrors and holders into single mode, polarization maintaining (PM) fiber optic cables terminated on both ends with a quarter-pitch gradient index (GRIN) lens. The GRIN lens restricts the k-vector of the collected light and focuses the beam to a 100 μm Gaussian waist. For Bragg scattering the optics produces an 8 mm collimated beam with a Gaussian profile that passes axially through the sample cell. Light scattered by the crystalline or crystallizing sample within the cell is focused by the hemispherical exit surface of the cell onto a concentric

fluorescent screen, while unscattered light is focused by the same optics onto a beam dump in the center of the screen. A CCD camera mounted on the far wall of the enclosure records a 10-bit image of the screen covering angles of 0-60°. The cable for dynamic light scattering directs the beam onto the parabolic skirt and through the center of the cell. The beam is totally internally reflected from the skirt radially through the sample. The two single-mode pick-up fibers, 180° apart, are attached to a motorized stage, allowing the scattered intensity to be collected at angles θ=10-169° with 0.1° resolution. A sensitive avalanche photodiode detector (APD) converts the scattered intensity into binary data from which two Brookhaven BI9000 correlators compute autocorrelation functions.

The sample cell is mounted into a circular holder, whose outer edge has ridges that grip a rubber belt that also hugs the gear of a PMI ServoDisc DC motor. The motor transmits sinusoidal oscillations at frequencies between 0.2 to 10 Hz to the sample cell through the rubber belt. Because our samples crystallize and, thus, are nonergodic, we ensemble average by rotating the cell slowly (<1°/minute) through many configurations.

DATA ANALYSIS

For nucleation and growth studies high resolution CCD images taken at regular intervals beginning shortly after shear melting of a sample quantify the growth of the Bragg peaks with 0.2° resolution. These are averaged azimuthally to obtain the intensity as a function of wavenumber and stored for analysis. The first step is to estimate the particle form factor $P(aq)$ and the instrument factor $\alpha(q)$ by dividing the intensity detected immediately after shear melting by the static structure factor $S_{py}(aq)$ for an equilibrium fluid at the appropriate volume fraction as approximated by the Percus-Yevick theory. Then for partially crystalline samples we obtain the static structure factor by dividing the measured intensity by $\alpha(q)P(aq)$. The contribution from the disordered fluid phase is then subtracted as $\beta(t)S_{py}(aq)$ with $\beta(t)$ chosen to bring the residual crystal structure factor $S_c(aq)$ to zero as q->0 (Figure 1a). Since $S_c(aq)$ generally reflects the random stacking of hexagonal planes, the main Bragg peak is accompanied by shoulders not present in the face-centered cubic structure (Figure 1b). Consequently the main peak is truncated at the shoulders and value of q at the maximum, the integral under the curve, and width at half maximum are recorded. These provide quantitative measures of the particle volume fraction within the crystallites, the crystalline fraction, and average crystallite size, respectively.

For the rheology measurements we obtain the autocorrelation function

$$g_1(q,\tau)=< E(q,0)E^*(q,\tau)>/<I(q,0)>$$

that decays from unity toward zero at a rate that depends on the driving frequency ω, the relaxation of the suspension without any forcing, and the response of the sample to the oscillatory forcing. If the sample were a rigid solid, $g_1(q,\tau)$ would be completely correlated at the inverse of the driving frequency or $\omega\tau=2\pi$ and would follow the shape of the forcing, i.e., sinusoidal. Since our sample is not totally rigid and we ensemble average by superimposing a slow rotation onto the oscillation, crystallites return close but not exactly to their original positions after one oscillation.

At shorter times, even for small amplitude oscillations, the angular rotation alone fully decorrelates the signal. Therefore, we measure the autocorrelation function at different driving frequencies at a scattering angle just off Bragg reflections and scale the delay time by the driving frequency and the amplitude of angular rotation to determine the resonant response. The detector sees the center of the sample, detecting the motion propagated inward from the boundaries and, therefore, the bulk rheological properties of the whole sample.

We extract the shear modulus G' and dynamic viscosity η' of our concentrated dispersions from solutions to the equation of the motion of a finite cylinder of a viscoelastic solid with radius and height R in oscillatory shear. The amplitude of the response at the center of the cylinder depends on the reduced frequency $\Omega=\omega R\,(\rho/G')^{1/2}$ and the reduced viscosity $\xi=\eta'/R(\rho G')^{1/2}$.

RESULTS

Nucleation and Growth

Reduction of the Bragg images during nucleation and growth as described above determines the time evolution of the average crystallite diameter $\langle L\rangle$ (from the width at half maximum), the crystalline fraction f (from the area under the primary Bragg peak), the number density of crystallites n_c (from the area divided by the crystallite volume), and the volume fraction ϕ_c within the crystallites (from the position of the Bragg peak). Figures 2 a-d display the results for one of the samples examined, positioned just below melting at $\phi = 0.552$. Since our analysis of the data is still in the early stages, we focus the following discussion on this sample, for which the trends are most clear.

The data from normal gravity suggests a critical nucleus L_c of 11-12 particle diameters. In microgravity we see three phases in the process. In Figures 1 a-c the initial slow transient for times $t < 150$ s is controlled by nucleation, while the period 150 s $< t <$ 300 s reflects diffusion-limited growth. When the crystalline fraction becomes significant, $f \cong 0.1$, the volume fraction within the fluid phase begins to drop, allowing that within the crystallites to relax toward melting or coexistence, i.e. ϕ_c -> 0.545. In the meantime, coarsening takes over and proceeds in two stages joined by a transition at roughly 6000 s. Note that the crystallites are significantly larger in microgravity, while the overall rate of crystallization remains the same. Presumably this indicates breakage of growing crystallites and leads to an over estimate of the rate of nucleation in normal gravity.

A simple model suffices to explain the nucleation and growth phase of this data. Assume the rate of nucleation to be constant and the rate of growth to be diffusion limited such that

$$n_c = \frac{dn_c}{dt}t \qquad \frac{dL^3}{dt} = \frac{L_c^2}{\tau}L$$

with τ the time scale for growth. From these the average crystallite size $\langle L\rangle$ and the crystalline fraction f follow as continuous functions of time with the limits

$$t/\tau << 1 \qquad f \approx L_c^3\frac{dn_c}{dt}t \qquad\qquad t/\tau >> 1 \qquad f \approx 0.07L_c^3\frac{dn_c}{dt}\frac{t^{5/2}}{\tau^{3/2}}$$

$$\langle L\rangle \approx L_c\left(1+\frac{4}{9}\frac{t}{\tau}+\ldots\right) \qquad\qquad \langle L\rangle \approx 0.8L_c\left(\frac{t}{\tau}\right)^{1/2}$$

These correspond qualitatively with the observed behavior

$$t/\tau << 1 \qquad f \propto t^{0.72} \qquad\qquad t/\tau >> 1 \qquad f \propto t^{2.24}$$

$$\langle L \rangle \propto t^{0.15} \qquad\qquad \langle L \rangle \propto t^{0.47}$$

though further analysis is needed to assess whether the magnitudes are reasonable relative to the predictions from classical and more sophisticated theory.

Rheology

The autocorrelation functions obtained during the small amplitude oscillations of an individual sample are normalized to one at early delay times and the delay times are scaled with the driving frequency. For each frequency, we then estimate the response of the sample to oscillatory shear by rescaling the delay time with a factor $\Lambda(\omega)/\Lambda(\omega_o)$ that collapses each onto the correlation function at the lowest measured frequency ω_o. Thus, the scaled correlation functions at the various driving frequencies should form a master curve. This works well for frequencies above 0.6 Hz so we force those correlation functions to coincide at g_1=0.5.

The response of Sample 4 as a function of driving frequency (Figure 3) for measurements made in normal and microgravity environments clearly exhibit the same resonance. Using the model, we choose $\Lambda(\omega_o)$, G', and η' so that the position and shape of the resonance best fit the data. The resonance frequency mainly determines the shear modulus G' and the amplitude and width control the dynamic viscosity η'.

For hard spheres the storage and loss moduli are naturally scaled as Ga^3/kT and η'/μ. Our measurements for the elastic moduli (Figure 4) compare well with the static shear moduli that Frenkel and Ladd (1987) obtained from simulations for an FCC crystal and lie well below the values predicted by Lionberger and Russel (1994) and measured by Shikata and Pearson (1994) for the metastable fluid. The static modulus is an equilibrium property that allows the structure to re-equilibrate to the applied strain and is unaffected by hydrodynamic interactions, while the high frequency modulus measures the instantaneous response to a strain. Consequently, the high frequency modulus always exceeds the static limit, though generally not by much for colloidal crystals. Thus our results are quite reasonable and agree with the measurements of van der Vorst, et al. (1995, 1996) on aqueous latex dispersions which also showed little variation in the modulus with frequency.

The dynamic viscosity scaled by the solvent viscosity exceeds both Nunan and Keller's (1984) calculations for the high frequency viscosity of an FCC crystal and the values measured by Shikata and Pearson (1994) and van der Werff, et al. (1989) for the metastable fluid. The high value may result from nonlinear effects. Frith, et al. (1987) found the loss modulus to pass through a maximum with increasing strain amplitude, while the storage modulus remained constant in the range of our measurements. If our strain amplitude lies near the maximum in the loss modulus, that would explain a higher value for the dynamic viscosity that falls close to the high shear limit for disordered dispersions.

CONCLUSIONS

Decomposition of the time-resolved Bragg peaks during nucleation, growth, and coarsening of hard sphere crystals at $\phi = 0.552$ suggests a constant rate of nucleation throughout the growth

period and diffusion-limited growth of the individual crystallites. Toward the end of growth the volume fraction within the crystallites relaxes toward the equilibrium value, as the volume fraction within the fluid falls toward the value at freezing. Coarsening also yields well defined trends but not ones that we are prepared to interpret. Gravity clearly affects the process reducing the crystallite size below that seen in microgravity and, thereby, leading to an over estimate of the number or density of crystallites. This may be responsible for significantly higher rates of nucleation deduced from laboratory experiments, relative to predictions from simple theories.

The resonance detected with dynamic light scattering gives reasonable values for the high frequency shear modulus of our colloidal crystals, representing the first data on viscoelastic properties of the nonaqueous hard sphere colloidal crystals. The high frequency dynamic viscosity seems a bit high, perhaps due to a nonlinear response. In this case the results for micro- and normal gravity are indistinguishable.

ACKNOWLEDGEMENTS

We thank the PHaSE team at NASA Lewis Research Center in Cleveland, OH for their work on the instrument and Sal Torquato for his advice on the orientationally averaged modulus. This research was funded by a NASA grant (NAG 3-1762) and Graduate Student Researchers Program Fellowship (NGT 3-52301).

REFERENCES

Benzing, D.W., and W.B. Russel *J. Colloid Interface Sci.* **83** 178 (1981).

Bolhuis, P., and D. Kofke *Phys. Rev. E* **54** 634 (1996).

Buscall, R., J.W. Goodwin, M. Hawkins, and R.H. Ottewill *J. Chem. Soc. Faraday Trans. I* **78** 2873 (1982).

Chen, L., B.J. Ackerson, and C.F. Zukoski **38** 193 (1994).

Chow, M., and C.F. Zukoski *J. Rheol.* **39** 33 (1995).

D'Haene, P. *Rheology of Polymerically Stabilized Suspensions* (Katholieke Universiteit Leuven, Netherlands, 1992).

Frenkel, D., and A. Ladd *Phys. Rev. Lett.* **59** 1169 (1987).

Frith, W., J. Mewis, and T. Strivens *Powder Technol.* **51** 27 (1987).

Frith, W., T. Strivens, and J. Mewis *J. Colloid Interface Sci.* **139** 55 (1990).

Harland, J.L., and W. van Megen *Phys. Rev. E* **55** 3054 (1997).

Harland, J.L., S.I. Henderson, S.M. Underwood, and W. van Megen *Phys. Rev. Lett.* **75** 3572 (1995).

He, Y., B.J. Ackerson, W. van Megen, S.M. Underwood, and K. Schatzel *Phys Rev. E* **54** 5286 (1996).

Krieger, I.M. *Adv. Colloid Interface Sci.* **3** 111 (1972).

Lant, C.T., A.E. Smart, D.S. Cannell, W.V. Meyer, and M.P. Doherty *Appl. Opt.* **36** 7501 (1997).

Lindsay, H., and P.M. Chaikin *J. Chem. Phys.* **76** 3774 (1982).

Lindsay, H., and P.M. Chaikin *J. Physique* **46** C3 (1985).

Lionberger, R.A., and W.B. Russel, *J. Rheol.* **38** 1885 (1994).

Mewis, J., W. Frith, T. Strivens, and W.B. Russel *AIChE J.* **35** 415 (1989).

Nunan, K., and J. Keller *J. Fluid Mech.* **142** 269 (1984).

Phan, S.-E., W.B. Russel, Z. Cheng, J. Zhu, P.M. Chaikin, J.H. Dunsmuir, and R.H. Ottewill *Phys. Rev. E* **54** 6633 (1996).

Pusey, P., and W. van Megen *An Exxon Monograph: Physics of Complex and Supermolecular Fluids*, (edited by S.A. Safran and N.A. Clark) John Wiley & Sons, New York, 1987, pp.673-698.
Schatzel, K., and B.J. Ackerson *Phys. Rev. E* **68** 337 (1992).
Schatzel, K., and B.J. Ackerson *Phys. Rev. E* **48** 3766 (1993).
Shikata, T., and D. Pearson *J. Rheol.* **38**, 601 (1994).
van der Werff, J., C.G. de Kruif, C. Blom, and J. Mellema *Phys. Rev. A* **39** 795 (1989).
van der Werff, J., and C.G. de Kruif *J. Rheol.* **33** 421 (1989).
van der Vorst, B., D. van den Ende, and J. Mellema *J. Rheol.* **39** 1183 (1995).
van der Vorst, B., D. van den Ende, and J. Mellema *Physica B* **228** 180 (1996).

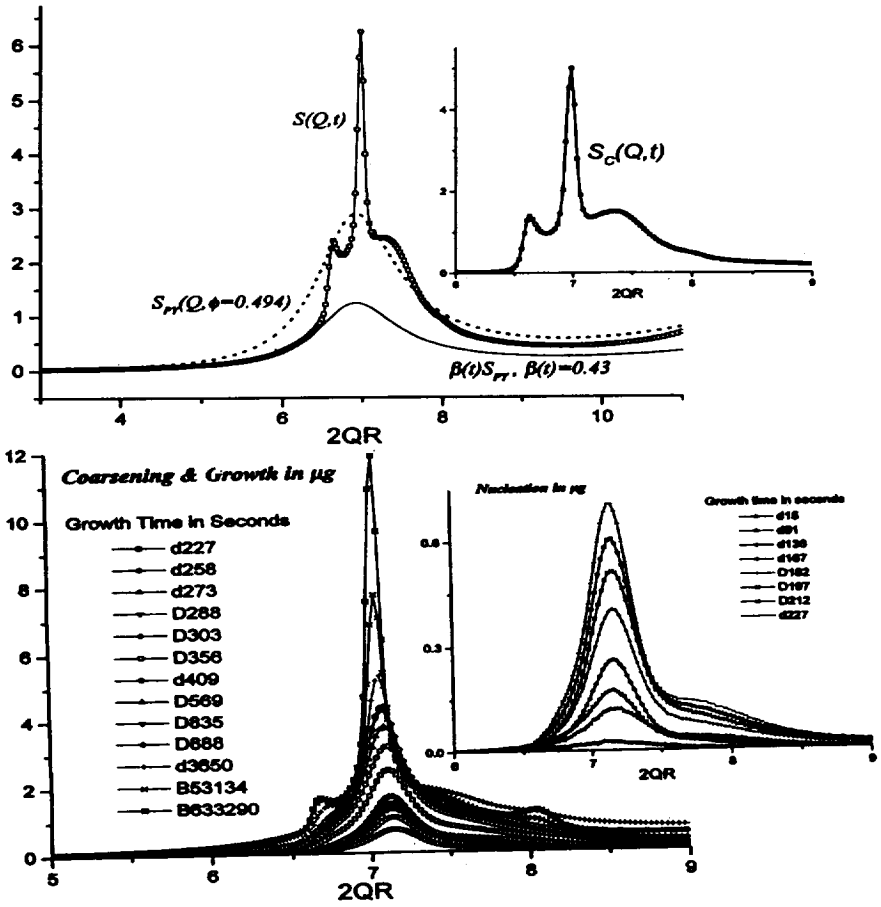

Figure 1 - Static structure factors for (a) a mixture of fluid and crystal demonstrating the subtraction of the corresponding S_{py} weighted by $\beta(t)$ and (b) the resulting structure factors for the crystallites at a series of times.

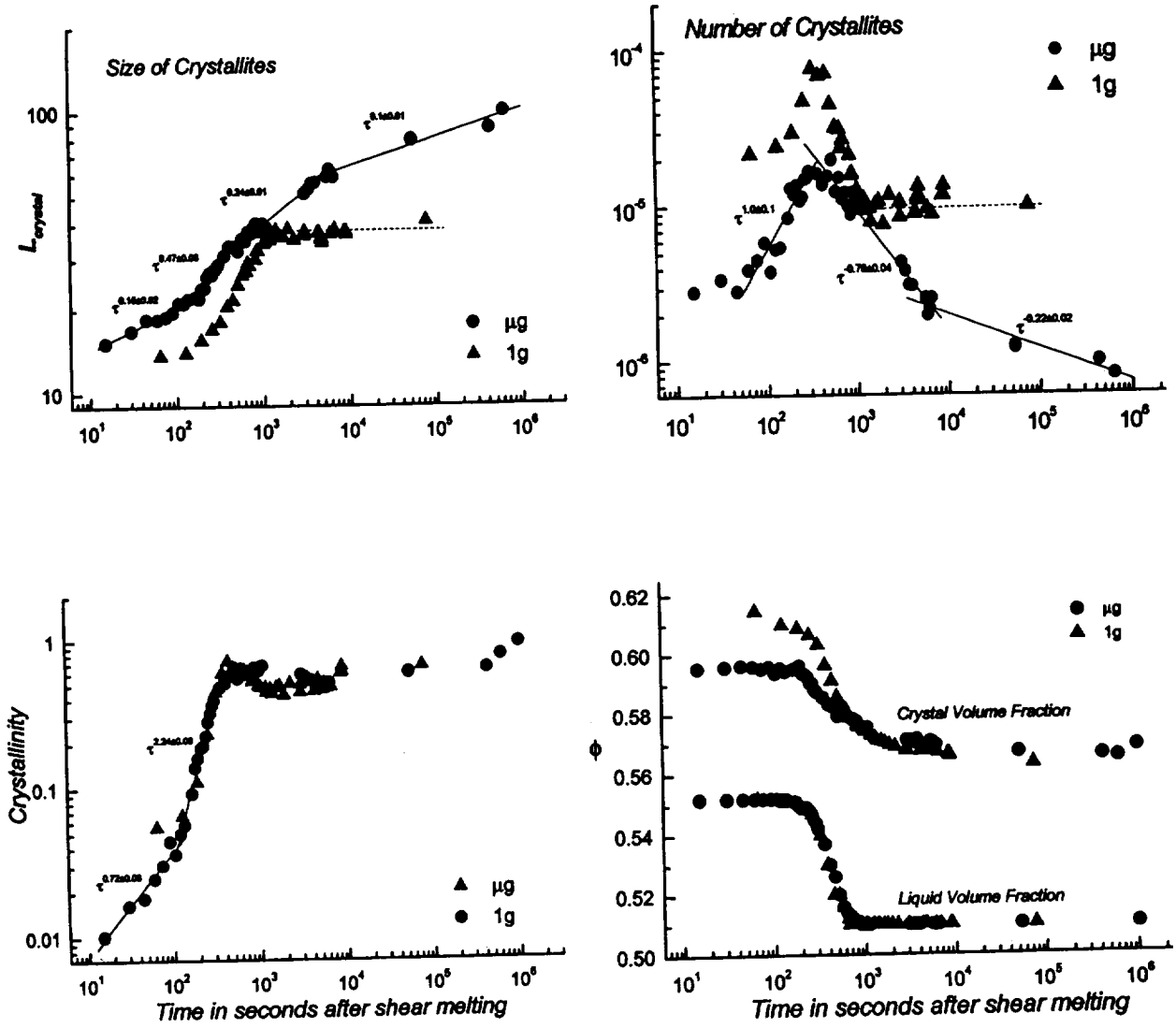

Figure 2 – The time evolution of (a) the average crystallite size <*L*>, (b) the crystalline fraction *f*, (c) the number density of crystallites $n_c = f/\langle L\rangle^3$, and (d) the volume fractions within the crystalline and fluid phases for $\phi = 0.552$.

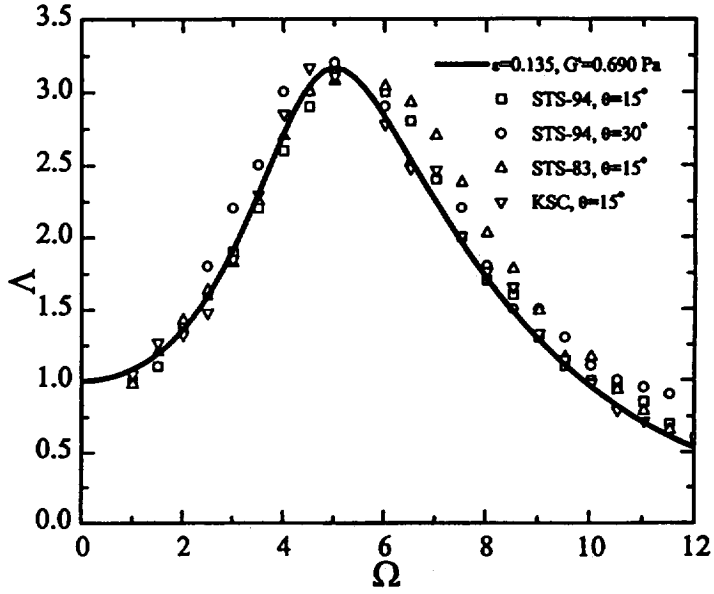

Figure 3 - Resonant response of Sample 4 STS-94 at various angles under gravity and microgravity vs driving frequency compared with the frequency independent model ξ=0.135.

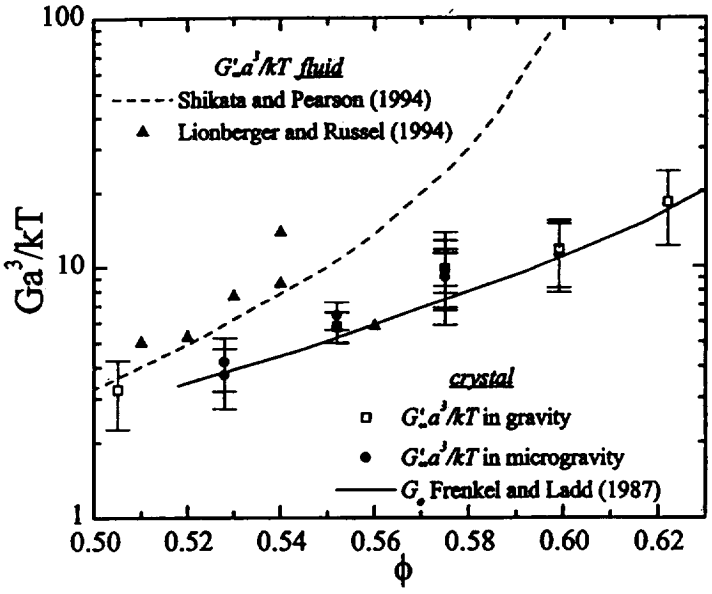

Figure 4 - The shear moduli of hard sphere crystals compared with measurements and theory for the high frequency moduli of the metastable fluid (Shikata & Pearson 1994, big triangleup; Lionberger & Russel 1994, - - -) and Frenkel and Ladd's prediction (1987, -----) for the static moduli of an FCC crystal.